TÜBİTAK

Turkish Journal of Earth Sciences

http://journals.tubitak.gov.tr/earth/

Research Article

Turkish J Earth Sci
(2016) 25: 81-101

doi:10.3906/yer-1503-3

Quartz-mica schist and gneiss hosted clay deposits within the Yenipazar (Yozgat, Central Anatolia) volcanogenic massive sulfide ore

Şıh Ali SAYIN*
Faculty of Engineering, Aksaray University, Aksaray, Turkey

Received: 02.03.2015 • **Accepted/Published Online:** 05.08.2015 • **Final Version:** 01.01.2016

Abstract: The Yenipazar deposit of volcanogenic sulfide occurrence, situated approximately 9 km SW of Yenipazar, is hosted in quartz-muscovite schists and gneiss. Following the Late Cretaceous, the quartz-mica schists and gneiss have been altered to clay minerals, resulting in important kaolin deposits. The clay deposits consist mainly of halloysite, kaolinite, smectite, illite, muscovite, chlorite, and α-quartz. Biotite, alunite, jarosite, pyrite, hematite, calcite, low cristobalite, and feldspar are present in minor amounts. In places, some mixed-layer clays, such as kaolinite/smectite and smectite/illite, are also observed within the clay deposits. Barite is present in a few clay samples. α-Quartz is the dominant silica mineral in all parts of the clay bodies, though silicification becomes more intense in an upward direction. Kaolinite and halloysite are the dominant clay minerals in the upper section of the clay deposits containing up to 36.10% Al_2O_3. At the middle and lower parts of the clay deposits, smectite and illite/mica are predominant. The Yenipazar clays are characterized by 41.80%–66.10% SiO_2, 16.80%–36.10% Al_2O_3, 2.10%–17.70% Fe_2O_3, 0.30%–6.20% MgO, 0.10%–5.70% CaO, 0.1%–0.70% Na_2O, and 0.10%–3.80% K_2O values. The silica gossan in the upper parts of the clay deposits and the mineral zonations reveal that hydrothermal alteration is the main cause for the development of the kaolin dominated clay deposits. Pb, Zn, Cu, Sr, Ba, and Zr enrichments and depletion of Cr, Nb, Ti, Ce, Y, and La within the clay deposits are supportive of the magmatic origin of the hydrothermal solution related to Late Cretaceous arc magmatism. Depletion of both total REEs and HREEs, as well as the enrichment of LREEs, in clay deposits refer to an altering acidic solution. The positive Eu and Ce anomalies indicate the presence of feldspar and Zr crystals in the clays, respectively. However, the data show that corrosive hot solutions, which might have arisen from magma, have played an important role in the kaolinization process together with hot meteoric waters. Scanning electron microscope investigations show that illite and smectite are the first minerals formed by the hydrothermal alteration of feldspar crystals.

Key words: Alunite, gneiss, halloysite, hydrothermal alteration, H metasomatism, jarosite, kaolinite, kaolinization, quartz muscovite schist, silica gossan, Yenipazar, Yozgat

1. Introduction

The rocks of the so-called Kırşehir Massif, consisting mainly of a metamorphic character, have been studied by numerous geologists since the early 1900s. Arni (1938) was the first geologist to study the crystalline rock series around the Kırşehir and Yozgat districts. According to Bailey and McCallien (1950), the Kırşehir Massif, which belongs to the Pontides, covers the Ankara Mélange. Erguvanlı and Buchardt (1954) prepared a geological map around the Kırşehir Massif at a 1:100,000 scale and identified all metamorphic rocks such as gneiss, mica schist, chlorite-sericite schist, amphibolites, calc-schist, and phyllite. Erkan (1975–1978, 1981) identified three metamorphic zones in the region. He emphasized that the degree of regional metamorphism has increased in the north and northeast directions. He concluded that this metamorphism formed at 5 kbar and 500–700 °C temperatures. Göncüoğlu (1977, 1981) investigated the southern part of the massif and after studying the mineral paragenesis in the region he concluded that regional metamorphism formed at 4–6 kbar and 600–650 °C temperatures. Seymen (1981–1984) pointed out that all metamorphic rocks in the region originated from the parent rocks: psammitic, semipelitic, orthoquartzitic, and carbonate rocks with chert. He also identified four metamorphic zones: greenschist facies, low amphibolite facies, high amphibolite facies, and amphibolite-granulite transition facies. Tolluoğlu (1986) identified three formations within the metamorphic zones, namely the Kalkanlıdağ formation, the Kargasekmez Tepe quartzitic member, and the Bozçaldağ formation in the region. The isograd positions of the fault systems have changed due to progressive metamorphism in the region (Erkan and Tolluoğlu, 1990).

* Correspondence: sasayin@gmail.com

Some private mining companies also carried out some mining activities and produced economical Cu-Pb-Zn minerals from the region. Sağıroğlu (1984) studied skarn-type Cu-Pb-Zn in the region. Following geological investigation, a private company discovered Cu-Pb-Zn mineralization in the study area (Figure 1). According to the geological studies, it is most probably a volcanogenic massive sulfide (VMS) deposit. In order to investigate the dimensions of the mineralization and its reserve, 145 diamond and 365 RC drill holes were opened in the study area. The mineralization zone was found to extend laterally in the S-N direction with a length of approximately 2000 m (Figure 1). After the examination of all drill hole samples, two clay bodies (clay deposits) approximately 400 and 550 m in length were observed in the northern and southern parts of the mineralization zone, respectively. In this study, clay samples from six representative drill holes opened in these parts were studied. These drill holes are ES3, YPD76, and ES4 in clay deposit A in the north and YPD140, YPD163, and YPD6 in clay deposit B in the south.

The aim of this study was to investigate the mineralogy, geochemistry, and modes of clay occurrences situated approximately 9 km SW of Yenipazar (Yozgat). The downhole and lateral variations of the clays were also observed in this area.

2. Materials and methods

Forty-seven clay samples taken from six drill holes were subjected to X-ray diffraction (XRD) analyses. All samples were prepared for powder and air-dried, solvated with ethylene glycol, and heated at 550 °C. The XRD analyses with a Rigaku Geigerflex (Japan) were carried out using CuKα-radiation with a scanning speed of 1° 2θ/min. Clay fraction samples of <2 μm in length were allowed to settle on glass slides. They were then air-dried, solvated with ethylene glycol at 60 °C for 2 h, and then heated at 550 °C for 2 h. Semiquantitative mineralogical determination of the clay samples was obtained by multiplying the intensities of the principal basal reflections of each mineral by suitable factors according to external methods developed by Gündoğdu (1982) after the method of Brindley (1980) and by combination of chemical analyses of the bulk samples. Thirty parent samples taken from the study area and boreholes were subjected to mineralogical and petrographic study. The mineralogy of these samples was determined by optical microscopy. Clay samples were also studied by optical microscopy in order to investigate the mineralogical composition.

Major oxides of 13 clay and two parent rock samples were determined by X-ray fluorescence spectrometry (Rigaku X-ray spectrometer RIX3000) using rock standards supplied by MBH Analytical Limited (United Kingdom) and Breitlaender (Germany). Clay samples were also subjected to trace element and rare earth element (REE) analyses by ICP with a Perkin-Elmer 4300 (USA).

For microstructure investigation, some representative clay samples were prepared for analysis with a scanning electron microscope equipped with EDX (FEI Quanta 400 MK; USA).

All experimental work was undertaken at the mineralogical and chemical analysis laboratories of the General Directorate of Mineral Research and Exploration (MTA) and Ankara University.

3. Geological setting

Figure 1 shows the geological map of the study area. In the region, the basement rocks are Paleozoic-Mesozoic aged metamorphic rocks, known as the Kırşehir Massif. The Kırşehir Massif consists of amphibolite, mica schist, gneiss, quartzite, and marble. The amphibolite originated from metaophiolite lenses (Erkan, 1980). In general, the marble unit is observed at the top of the Kırşehir Massif. Seymen referred to the marble unit and the rest of the metamorphic rocks as the Boğazçaldağ Formation and the Kalkanlıdağ Formation, respectively (1981). These formations were controlled by Alpine metamorphism under the condition of amphibolite facies (Kurt et al., 1991). In the study area, metamorphic rocks are identified as quartz-muscovite schist, gneiss, and marble. The quartz-muscovite schist and gneiss mainly consist of quartz, muscovite, and feldspar with lepidogranoblastic texture. Quartz and muscovite crystals occur in alternating bands. Granoblastic and granofibroblastic textures are also observed in some mica schists and gneisses. Biotite is present in some samples. The Kırşehir Massif was unconformably overlain by cherts, sandstone, and claystone and mudstone lens-bearing limestone of Early Eocene age. The limestones show thick bedding and are yellowish, light gray, and brownish. Outside of the study area, to the north, the Lutetian aged Beycedere Formation consisting of nummulitic limestones with interbedded sandstone and claystone lenses overlies this limestone unit. The Beycedere Formation was overlain with angular discordance by the Oligocene aged Kızılöz Formation consisting of interbedded reddish pebble stones and yellow-green colored claystones. The Neogene aged Kızılırmak Formation, which mainly consists of sandstones with pumice pebbles, claystones, marl, tuffs, tuffites, and white-gray thick limestone, outcrops widespread in the region. The bottom of the formation is mainly represented by pumice pebble-bearing yellow-green sandstones. Claystones, marls, tuffs, and tuffites are present in the middle of the formation. Yellowish white and light gray medium-thick bedded limestones dominate the upper section of the formation. The fossils indicate that these sediments were deposited in a lake environment during the Late Miocene-Pliocene (Kurt et al., 1991).

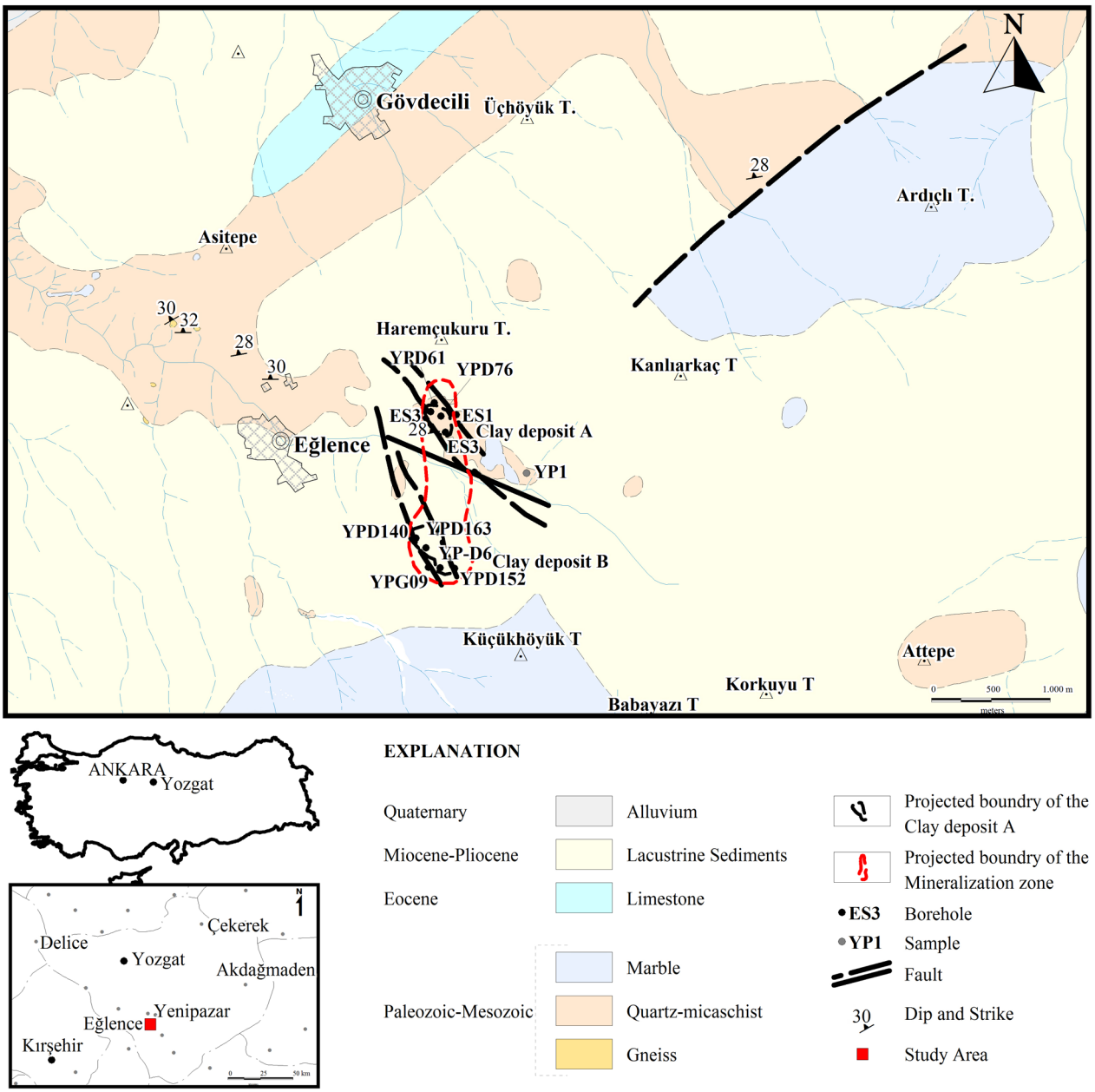

Figure 1. Geological map of the study area (compiled from Kurt et al., 1991).

Quaternary aged alluvium, which consists of uncemented conglomeratic lacustrine limestones, metamorphic rocks, and granitic and ophiolitic rocks from silt to rounded large pebbles, is present only as a small outcrop in the northwest corner of the study area.

Kurt et al. (1991) pointed out that orogenic cycles with compression and extension continued just after Late Cretaceous and Paleocene magmatic activities. The presence of drifted Eocene transgressive sediments within the extensional graben system has emphasized transform faults and block rotations. The magmatic activities that originated from the crust indicate that the orogenesis persisted during Early Cretaceous-Paleocene geological times (Bayhan and Tolluoğlu, 1987). Ophiolites together with flysch overlying the Kırşehir Massif were intruded by a granite unit during the Uppermost Cretaceous. It implies a paroxysmal phase of orogenesis in the Upper Cretaceous-Paleocene (Akyürek et al., 1984). In general, the Kırşehir Massif has been cut by granitic and syenitic intrusive rocks in the east and north. In addition to the Kırşehir Massif, ophiolites have also been cut by granitic, syenitic, and pegmatitic rock series. All units in the region

are overlain by Eocene aged transgressive sediments. Kurt et al. (1991) suggested that there is a relation between these transgressions and the transform faults that occurred during the last period of collision. They came to the conclusion that the mantle originated magmatic activities could represent arc magmatism, or that these magmatic activities may have occurred a result of an extensional regime associated with transform movements.

According to the synthesis of Oczlon (2006), preceding Late Cretaceous northward subduction of the Tethys Ocean resulted in arc magmatism that created the Pontide copper belt with numerous VMS deposits. Mid-Late Cretaceous subduction also took place within the Tethys Ocean, causing the collision around the margins of the Central Anatolian microcontinent on which the Yenipazar VMS Orebody is located (Figure 2). Here, the age of metamorphism is zircon-dated at 91–84 Ma (Whitney et al., 2003), followed by the intrusion of a large granitoid massif at about 77–74 Ma (Whitney and Hamilton, 2004). These activities took place during the middle part of the Late Cretaceous, before the accretion of Central Anatolia to northern Turkey.

4. General features of clay occurrences

No clay outcrops are seen at the surface. In other words, all clay occurrences have been observed by drilling activities done for investigation of the Pb-Zn-Cu ore body in the study area. After studying all of the core samples, two clay deposits were observed in the northern and southern part of the mineralization area, namely clay deposit A in the north and clay deposit B in the south. All clay studies are based on samples taken from the representative six drill holes opened on these clay deposits. Drill holes ES3, YPD76, and ES4 with 122, 129, and 132 m depths in the north and drill holes YPD140, YPD163, and YPD6 with 163, 70, and 142.5 m depths in the south, respectively, are shown in Figure 1. The clay deposit consists of several clay veins in different thicknesses within the slightly altered quartz-muscovite schist and gneiss and mineralization zones (Figure 3).

4.1. Drill hole ES3

Drill hole ES3 is a massive sulfide-bearing mica schist outcrop about 12 m thick at the surface, partly altered. Clay and weakly clay veins are observed with thicknesses of 18 and 14 m, respectively, below this mica schist.

The clay vein is about 18 m thick and consists of kaolinite, illite/mica, smectite, alunite, jarosite, quartz, and feldspar in the upper section of the zone. The dominant clay is gray kaolinite. Kaolinite, halloysite, illite/mica, smectite, quartz, alunite, and jarosite are present at the middle of the zone. Kaolinite and halloysite are the dominant clay minerals. The clay is gray and light green. Smectite, halloysite, illite/mica, quartz, calcite, and feldspar are observed in the lower section of the zone. Smectite is the dominant clay. The clay is green, reddish, and pinkish.

The weakly clay vein is about 14 m thick and consists mainly of illite/mica, chlorite, smectite, mixed-layer clay, kaolinite, quartz, calcite, feldspar, alunite, hematite, and pyrite in the upper section of the zone. Chlorite, illite/mica, smectite, mixed-layer clay, quartz, calcite, feldspar, alunite, and hematite are observed in the lower section of the zone. Here, chlorite and illite/mica are the dominant minerals. The clay is green.

4.2. Drill hole YPD76

Neogene lacustrine sediments are present at the surface. Below this formation is slightly altered muscovite schist 1 m in thickness. Between this unit and the bottom of the drill hole, two clay veins are observed with thicknesses of 2 m.

Clay vein 1 is 2 m thick and consists of kaolinite, smectite, illite/mica, feldspar, quartz, hematite, and barite. Here, the dominant clay is white and pinkish kaolinite.

Clay vein 2 is 2 m thick and consists of smectite, kaolinite, illite/mica, chlorite, quartz, feldspar, hematite, and barite. Here, the dominant clay is smectite.

4.3. Drill hole ES4

At the surface, silicified and slightly altered quartz-muscovite schist with a thickness of 14 m is present. Two clay and two weakly clay veins are observed with thicknesses of 8, 14, 12, and 8 m, respectively, between the quartz-muscovite schist and the bottom of the drill hole.

Clay vein 1 is about 8 m thick and consists of kaolinite, smectite, illite/mica, calcite, quartz, and feldspar. Here, yellowish and gray kaolinite is the dominant clay.

Clay vein 2 is about 14 m thick and consists of smectite, kaolinite, illite/mica, feldspar, and quartz. Here, gray smectite is the dominant clay.

Weakly clay vein 1 is about 12 m thick and consists of mixed-layer clay, illite/mica, chlorite, quartz, feldspar, calcite, and pyrite.

Weakly clay vein 2 is about 8 m thick and consists mainly of illite/mica, smectite, chlorite, quartz, feldspar, calcite, and hematite. Here, illite/mica, smectite, and chlorite are the dominant minerals. The clay is mainly green.

4.4. Drill hole YPD140

Neogene lacustrine sediments called the Kızılırmak Formation are present at the surface with a thickness of 2 m. Between the Neogene lacustrine sediments and the bottom of the drill hole, two clay veins are observed with thicknesses of 2 and 18 m, respectively.

Clay vein 1 is 2 m thick and consists of kaolinite, smectite, illite/mica, quartz, alunite, and chlorite. Here, the dominant clay is white kaolinite.

Clay vein 2 is about 18 m thick and consists of kaolinite,

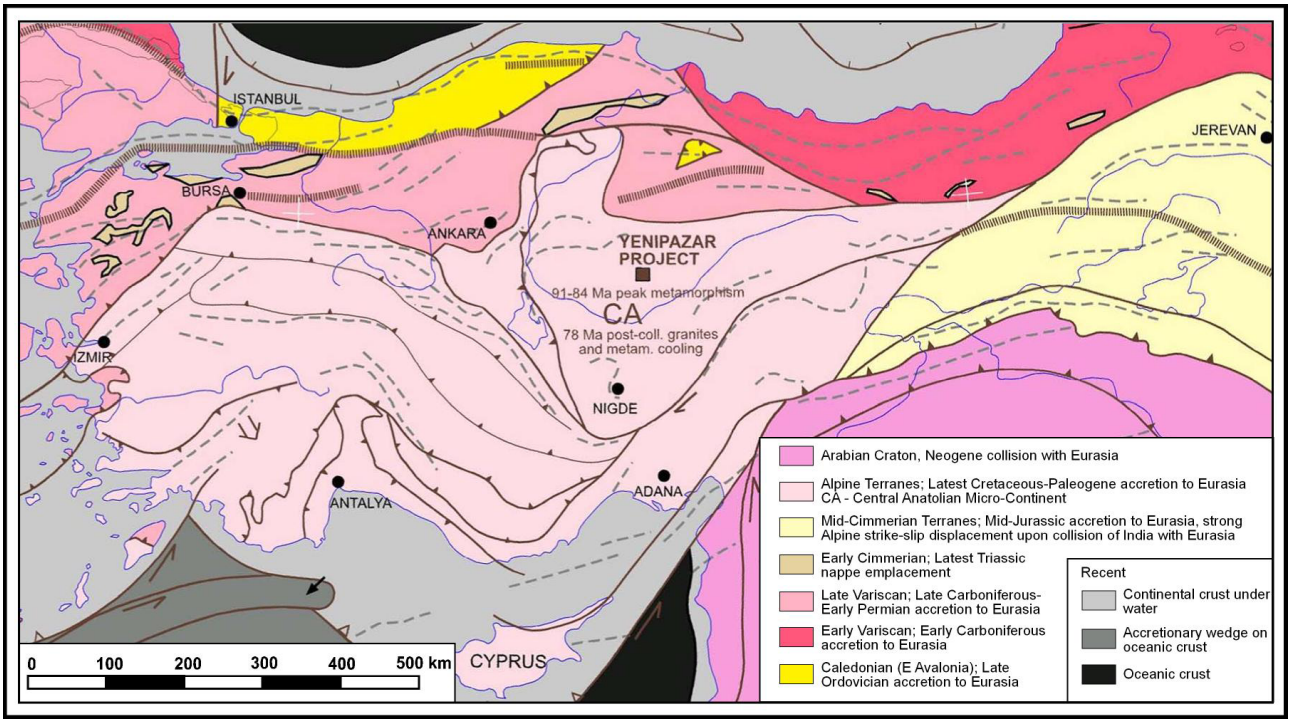

Figure 2. Regional terrain map of Turkey (from Oczlon, 2006).

smectite, mixed-layer clay, illite/mica, quartz, alunite, jarosite, goethite, and hematite in the upper section; smectite, illite/mica, kaolinite, alunite, jarosite, quartz, and hematite in the middle section; and illite/mica, smectite, kaolinite, alunite, quartz, feldspar, and hematite in the lower section of the zone. Here, the dominant clays are reddish and consist of kaolinite and smectite.

4.5. Drill hole YPD163

Neogene sediments are present at the surface with a thickness of 13 m. Two clay veins are present between the Neogene lacustrine sediments and the bottom of the drill hole.

Clay vein 1 is about 4 m thick and consists of kaolinite, mixed-layer clay, chlorite, illite/mica, quartz, alunite, jarosite, and feldspar in the upper section and kaolinite, smectite, illite/mica, quartz, alunite, and feldspar in the lower section of the zone. Here, the dominant clay is white kaolinite.

Clay vein 2 is 3 m thick and consists of kaolinite, illite/mica, smectite, quartz, and hematite. Here, the dominant clay is white kaolinite.

4.6. Drill hole YPD6

Neogene lacustrine sediments are present at the surface with a thickness of 10 m. Just below this formation, a silica zone about 2 m thick is observed. Between the silica zone and the bottom of the drill hole, four clay veins and three weakly clay veins are observed in varying thicknesses of about 3, 1, 3, 5, 5, 5, and 2 m, respectively.

Clay vein 1 is about 3 m thick and consists of kaolinite, illite/mica, smectite, quartz, feldspar, and calcite. Here, the dominant clay is kaolinite. The clay is white in the upper section but becomes yellowish in the lower section.

Clay vein 2 is about 1 m thick and consists of kaolinite, smectite, mixed-layer clay, quartz, and alunite. Here, the dominant clay is white and greenish kaolinite.

Clay vein 3 is about 3 m thick and consists of halloysite, smectite, illite/mica, and quartz. Here, the dominant clay is light green halloysite.

Clay vein 4 is about 5 m thick and consists of halloysite, illite/mica, mixed-layer clay, quartz, low cristobalite, calcite, and alunite in the upper section and kaolinite, illite/mica, smectite, chlorite, quartz, alunite, and calcite in the lower section of the zone. Here, the dominant clays are halloysite and kaolinite. The clay is white and light green at the top, but reddish at the bottom of the zone.

Weakly clay vein 1 is about 5 m thick and consists of illite/mica, chlorite, smectite, quartz, and low cristobalite. Here, the dominant clays are illite/mica and smectite. The clay is greenish in at the top, but yellowish at the bottom of the zone.

Weakly clay vein 2 is about 5 m thick and consists of illite/mica, chlorite, kaolinite, quartz, pyrite, hematite, feldspar, and alunite. Here, illite/mica and chlorite are the dominant minerals. The clay is mainly gray, light green, and reddish.

Weakly clay vein 3 is about 2 m thick and consists of illite/mica, chlorite, smectite, quartz, feldspar, alunite,

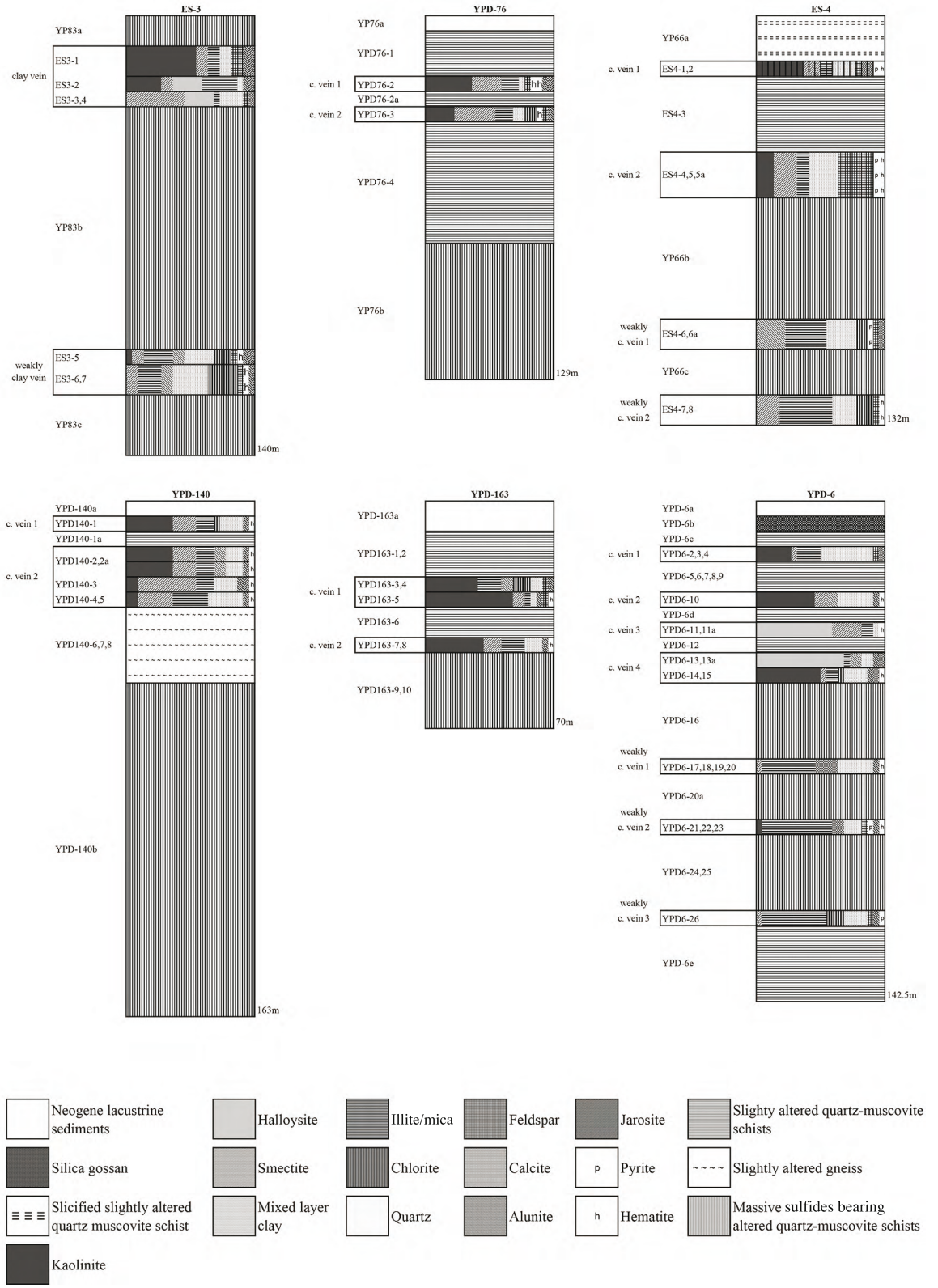

Figure 3. Schematic representation of the samples from the Yenipazar clay deposits on the basis of the semiquantitative XRD analyses.

and pyrite. Here, illite/mica and chlorite are the dominant minerals. The clay is mainly green.

5. Results

5.1. Petrographic determinations

Muscovite schists are abundant in the study area, while gneisses occur in lesser amounts as parent rocks. Muscovite schist mainly consists of muscovite, quartz, and feldspar with lesser amounts of biotite, chlorite, and opaque minerals (Figure 4a). Some samples comprise sillimanite and disthene crystals (Figures 4b and 4c). All phenocrysts are characterized by banding. Carbonation is common between phenocrysts. Chloritized mineral relicts are present in some samples. The rocks show

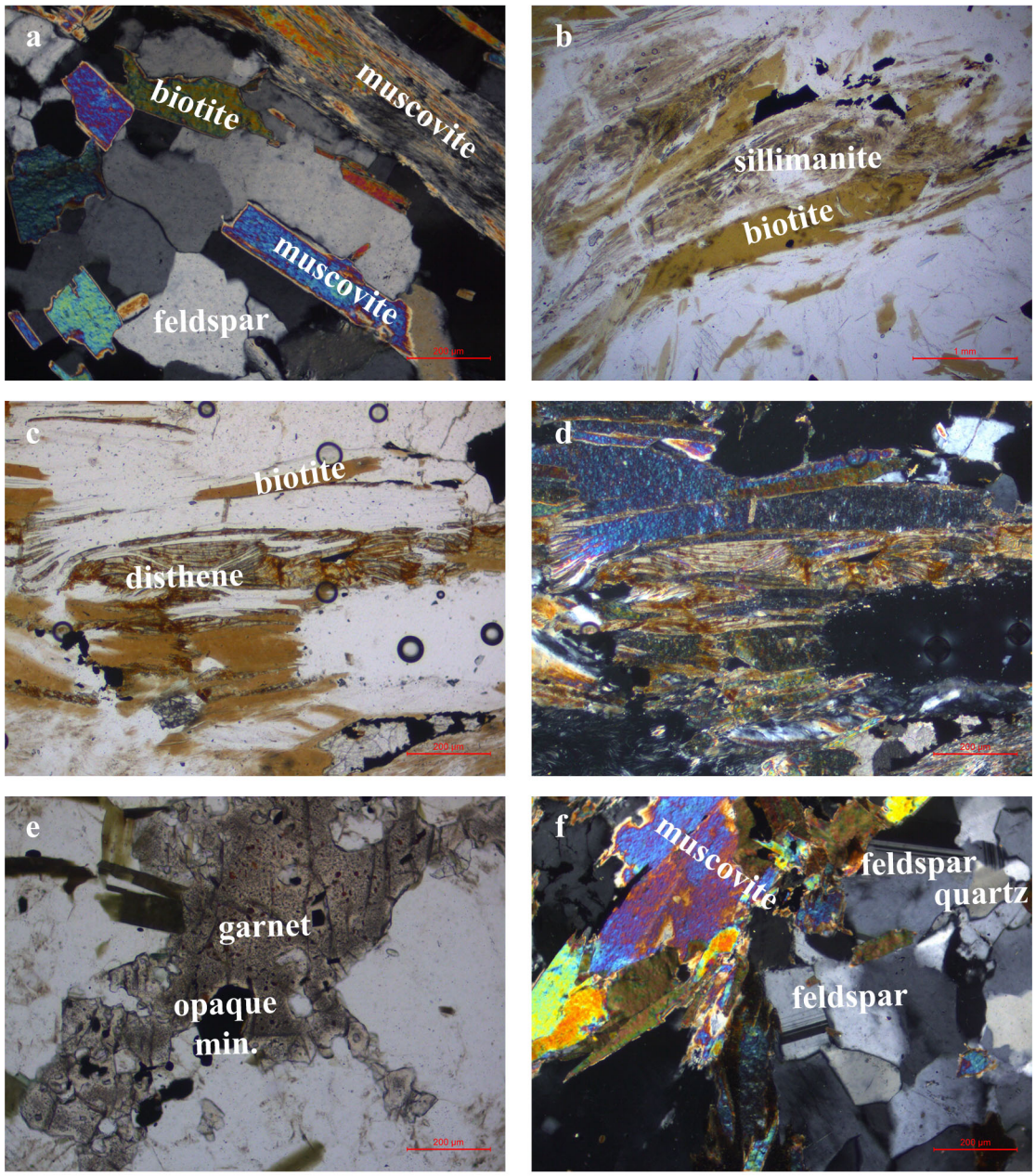

Figure 4. Photomicrographs showing: a) muscovite schist having granoblastic texture, cross-polar (YPD76-5); b) sillimanite crystal within muscovite schist, plane-polarized light (YPD163-6); c) disthene crystals within muscovite schist, plane-polarized light (YPD6-27); d) muscovite schist having fibrogranoblastic texture, cross-polar (YPD6-27); e) garnet crystals within muscovite schist, plane-polarized light (ES4-3); f) gneiss having granoblastic texture, cross-polar (YPD140-6).

mainly lepidogranoblastic texture, but granoblastic and granofibroblastic textures are also observed in some samples (Figure 4d). Gneiss consists of muscovite, quartz, feldspar, and biotite phenocrysts. Some feldspar crystals are both argillized and carbonatized. Garnet and some opaque minerals such as pyrite are seen in most samples (Figure 4e). Granoblastic texture is dominant in gneisses (Figure 4f).

5.2. XRD determinations

The XRD patterns of clays taken from the six boreholes show that the clay deposits consist of kaolinite, halloysite, smectite, illite, mixed-layer clay, muscovite, biotite, chlorite, quartz, low-cristobalite, calcite, feldspar, pyrite, alunite, jarosite, hematite, and barite. From the thin section studies, muscovite and biotite within some clay samples are clearly observed. On the other hand, illite and micas show almost identical X-ray reflections in the XRD patterns. Due to difficulties in distinguishing both illite and micas, the usage of the illite/mica symbol is generally accepted. Kaolin group minerals are dominant in the upper section of the clay bodies (Figure 3), whereas in the center and towards the lower part of the clay bodies, smectite and illite are predominant minerals. Mixed-layer clay minerals such as kaolinite/smectite and smectite/illite are observed in a some samples. Quartz is observed in all clays. Low cristobalite is seen in a few samples in small amounts. Most samples contain alunite and jarosite in minor amounts. Chlorite is mainly widespread within the lower part of the clay occurrences. Calcite occurs in a few samples in the lower part of the clay deposits. Pyrite and hematite are rarely present in the clays. Barite is observed in only samples YPD76-2 and YPD76-3.

For detailed studies on clay minerals, in addition to powder analyses, air-dried, ethylene-glycolated, and heated (550 °C) samples were prepared for XRD studies (Figure 5). XRD patterns of the clays show that, except for Sample 4-2, which has a value of 1.53 Å at the (060) (hkl) surface, indicating a trioctahedral smectite, probably saponite, the rest have 1.49 Å and 1.50 Å (060) values, indicating dioctahedral smectite.

5.3. SEM determinations

SEM studies of some selected samples from the clay deposits can be summarized as follows (Figure 6). Well-formed hexagonal and crudely shaped kaolinite crystals up to 20 μm in diameter are tightly packed, having a massive appearance. Based on SEM investigation, the porosity of the clay sample is very low (sample ES3-2, Figure 6a). Tube-shaped halloysite crystals up to 1.5 μm in length show tight packing. The porosity of the clay sample is very low (sample YPD6-11A, Figure 6b). Tube-shaped halloysite crystals gather to form a large flock. This micrograph represents in situ alteration of feldspar crystals (sample YPD6-13, Figure 6c). Clusters of halloysite tubes, which are associated with kaolinite plates, suggest a phase transition between halloysite and kaolinite (sample YPD6-11, Figure 6d). Very tiny kaolinite crystals (0.5 μm in diameter) appear to have formed on the pseudorosette texture of montmorillonite crystals (sample YPD6-19, Figure 6e). Curly montmorillonite crystals represent autogenic alteration of mica schist (sample ES3-4, Figure 6f).

5.4. Geochemistry

In this section, the major oxides of the geochemistry of the parent rocks and clays will be evaluated. The geochemistry of the trace elements and REEs of the parent rocks and clays will be discussed in Section 6.3.

Representative chemical analyses of two parent rock samples, fresh (YPD76-5) and slightly altered (YPD6-27) quartz-muscovite schists, and related clay samples are given in Table 1. The SiO_2, Al_2O_3, Fe_2O_3, MgO, K_20, CaO, and S values in the parent rocks reflect the presence of muscovite, quartz, feldspar, biotite, chlorite, calcite, pyrite, garnet, sillimanite, and disthene. There is a decrease in SiO_2, K_2O, and MgO and an increase in Al_2O_3, Na_2O, and LOI from parent rock samples to samples of clay deposits. The high Al_2O_3 and LOI and low SiO_2 values in the clay units imply the strong kaolinization ±smectite ±illite/mica. In addition, presence of sulfate minerals, namely alunite and jarosite in the clays, yields high LOI values. Due to breakdown of parent rock minerals during kaolinization, depletion of Mg^{+2} and K^+ gives rise to low MgO and K_2O values in the clay deposits. The parent rocks and clay samples both contain considerable amounts of Fe_2O_3.

The chemical analyses of the clays show that the Al_2O_3 content varies from 13.20% to 36.10%. In general, there is a positive relation between Al_2O_3 content and intensity of kaolinization; higher Al_2O_3 content indicates more kaolinization. It is seen from Figure 3 and Table 2 that kaolinite and halloysite are the dominant clay minerals present in the upper section of the clay bodies, indicating intensive kaolinization with 28.30%, 29.70%, and 34.70%, and 36.0% and 36.10% of Al_2O_3 values. Meanwhile, the 13.20%, 16.80%, and 19.40% Al_2O_3 content in the lower part of the clay deposits indicates a low level of kaolinization, since here smectite, illite/mica, and chlorite are predominant. A considerable amount of MgO content such as 6.0% and 6.2% within the clays is attributed to chlorite and smectite. In all clays, the Na_2O content varies from <0.1% to 0.7% and may be attributed to the presence of plagioclase. The K_2O content, which varies from 0.1% to 3.8%, is related to illite, muscovite, biotite, K-feldspar, jarosite, and alunite. The CaO content varies from 0.1% to 6.0% and is mainly attributed to smectite, plagioclase, and calcite. Especially samples taken from borehole ES4 (ES4-2, ES4-6, and ES4-7) contain a considerable amount

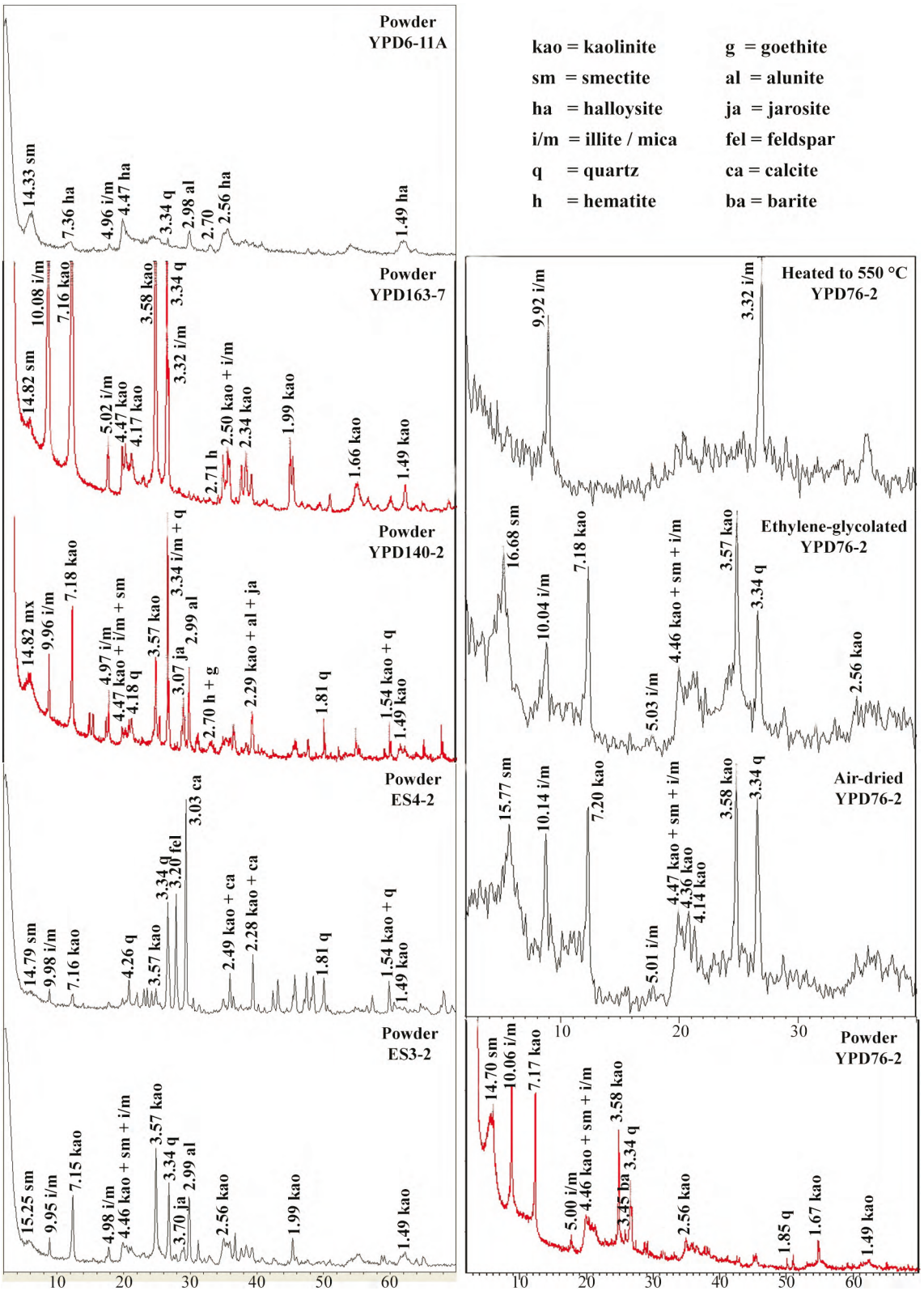

Figure 5. X-ray diffraction patterns of selected samples from the Yenipazar clay deposits.

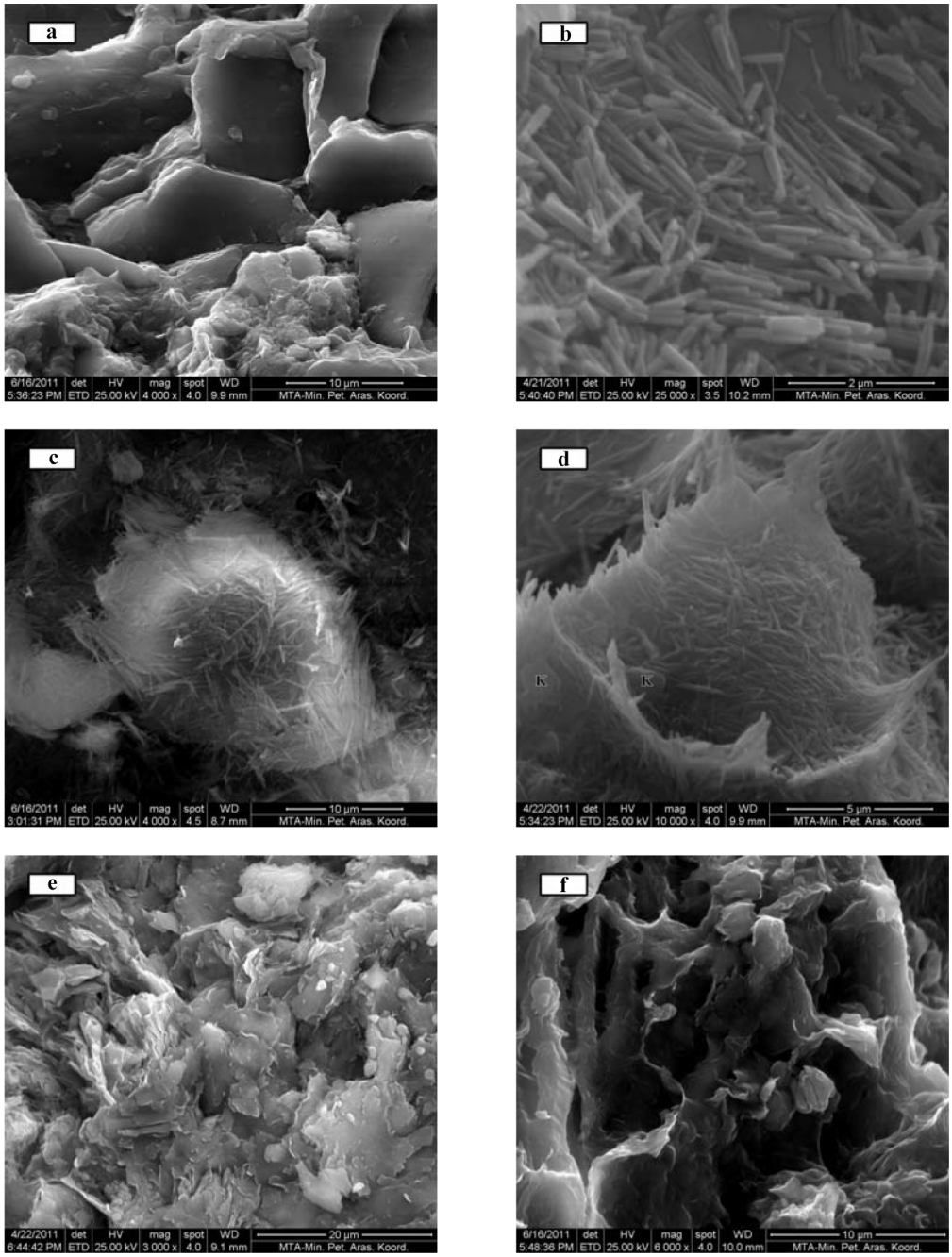

Figure 6. SEM images of clays: a) large hexagonal and crudely shaped kaolinite crystals tightly packed in sample ES3-2; b) very small tube-shaped halloysite crystals show rather tight packing in sample YPD6-11A; c) tube-shaped halloysite crystals gathered to form a large flock in sample YPD6-13; d) cluster of tube-shaped halloysite crystals are associated with kaolinite plates in sample YPD6-11; e) very small kaolinite plates appear to have formed on the pseudorosette texture of montmorillonite crystals in sample YPD6-19; f) curly montmorillonite crystals in sample ES3-2. K: kaolinite.

of calcite. The total iron values, which range from 2.1% to 17.90%, are mainly related to iron minerals, mainly pyrite, hematite, and goethite. On the other hand, a small amount of iron could be found in the structure of clay minerals, chlorite, feldspar, and jarosite. Sulfur contents varying between 0.10% and 3.05% are related to pyrite, alunite, jarosite, and barite. Due to a considerable amount of associated silica minerals, mainly quartz and

Table 1. Major oxide (wt.%) and trace element (ppm) analyses of two parent rock samples (YPD76-5 and YPD6-27) and representative samples from the Yenipazar (Yozgat) clay deposits.

Sample	YPD76-5	YPD6-27	ES3-4	ES3-5	YPD76-2	YPD76-3	ES4-2	ES4-6
Major oxides (wt.%)								
SiO_2	59.42	61.24	58.7	57.7	42	51.5	56.1	66.1
TiO_2	0.01	0.35	0.4	0.3	0.4	0.4	0.2	0.3
Al_2O_3	19.53	19.42	24.5	19.4	28.3	25.8	19.8	16.8
Fe_2O_3	6.25	7.4	3.8	5.1	9.8	5.7	3.4	2.7
MgO	4.6	3.98	1.3	3.2	1.2	0.9	6.2	2.5
CaO	0.65	0.13	1.3	0.6	0.6	0.6	6.0	2.55
Na_2O	0.04	0.04	<0.10	<0.10	<0.10	0.3	0.7	0.4
K_2O	6.2	3.98	0.4	2.7	0.8	1.3	2.1	1.9
MnO	0.14	0.26	<0.10	0.1	<0.10	<0.10	0.2	0.1
P_2O_5	0.05	0.06	0.1	<0.10	<0.10	0.1	<0.10	<0.10
LOI	1.83	1.63	8.65	10.15	11.0	7.95	5.0	5.25
Total	98.79	98.09	99.35	99.45	94.4	94.65	99.8	98.4
S	0.42	0.69	0.21	2.38	0.6	0.55	0.33	0.11
Trace elements (ppm)								
Pb	88	33.9	1120	720	4266	11900	1780	1520
V	33	43	4	4	45	20	6	3
Co	17	29.5	<1.00	1	10	5	1.5	2
Ni	18	1.9	6	5	7	8	8	9
Cu	13.5	14.5	680	594	1170	1285	940	882
Zn	447	623	740	33	3890	3540	635	520
Se	<1.00	<1.00	<1.00	<1.00	<1.00	<1.00	<1.00	<1.00
Sr	34.4	44.8	519	466	171	269	141	241
Y	18.1	41.8	8	4	5	2	4	5
Cd	13	1.7	<1.00	1	<1.00	3	<1.00	1
La	125.9	27.7	25	8	6	2	23	10
Ba	6640	834	420	680	25700	22000	790	1750
Cr	25	39	11	11	12	16	36	11
Rb	147	146	49	16	47	112	12	30
Zr	353	284	502	294	414	588	212	478
Nb	50	24	30	12	32	38	17	30
Ce	104	73	168	209	53	151	108	167
Pr	10	0.4	0.6			0.7	1.6	
Nd	16	2	2			3	6	
Sm	2.9	0.4	0.4			0.7	1.3	
Eu	4.1	0.2	0.5			1.1	0.6	
Gd	6.7	0.7	1.3			2.3	1.6	
Tb	0.4	0.1	0.1			0.1	0.2	
Dy	1.7	0.3	0.1			0.8	0.7	
Ho	0.3	0.1	0.1			0.1	0.1	
Er	0.9	0.1	0.2			0.4	0.4	
Tm	0.1	0.1	0.1			0.1	0.1	
Yb	1.1	0.1	0.2			0.5	0.3	
Lu	0.2	0.1	0.1			0.1	0.1	
∑REE	274.3	105.3	198.7			162.9	144	
$(Eu/Eu)_{)cn}$	2.84	1.16	2.12			2.65	1.27	
$(Ce/Ce)_{)cn}$	1.1	0.91	1.47			1.83	1.07	
$(La/Sm)_{)cn}$	9.11	3.15	4.72			2.7	6.77	
$(La/Yb)_{)cn}$	25.74	13.48	10.11			4.05	31.46	
$(La/Lu)_{)cn}$	677.42	64.52	96.77			96.77	451.61	
$(Eu/Sm)_{)cn}$	3.75	1.33	3.32			4.17	1.22	
$(Gd/Yb)_{)cn}$	4.92	5.65	5.25			3.71	4.3	
$(Tb/Yb)_{)cn}$	1.6	4.41	2.2			0.88	2.94	
$(Tb/Lu)_{)cn}$	1.36	0.68	0.68			0.68	1.36	

Table 1. (Continued.)

Sample	ES4-8	YPD140-2	YPD163-5	YPD163-7	YPD6-10	YPD6-13A	YPD6-23
Major oxides (wt.%)							
SiO_2	54.8	41.8	43.1	45.6	53.5	44.1	57.2
TiO_2	0.2	0.3	0.3	0.4	0.3	0.5	0.3
Al_2O_3	19.5	17.7	36	34.7	29.7	36.1	19.4
Fe_2O_3	3.3	17.8	1.6	3.2	3.7	2.1	6.5
MgO	6	0.5	0.3	2.3	0.7	1.2	3.3
CaO	5.7	0.3	0.2	0.2	0.7	0.2	0.1
Na_2O	0.7	0.2	<0.10	0.1	0.1	0.1	0.1
K_2O	2.1	1.8	0.5	1.8	0.5	0.1	3.8
MnO	0.2	<0.10	<0.10	<0.10	<0.10	0.1	0.1
P_2O_5	<0.10	<0.10	<0.10	<0.10	<0.10	0.1	0.1
LOI	7.85	15.35	15.55	11.25	9.8	13.65	7.95
Total	100.45	95.95	97.85	99.75	99.2	98.25	98.85
S	0.18	2.47	1.75	0.1	0.38	0.38	3.05
Trace elements (ppm)							
Pb	1340	21695	905	257	2490	4210	1150
V	4	10	8	15	6	6	6
Co	<1.00	3	3	1	<1.00	<1.00	<1.00
Ni	9	8	2	3	5	1	<1.00
Cu	204	3575	237	103	1933	784	915
Zn	365	7300	213	118	1283	802	4080
Se	<1.00	<1.00	<1.00	<1.00	<1.00	<1.00	<1.00
Sr	250	528	387	397	247	247	199
Y	7	5	2	4	4	4	18
Cd	<1.00	3	<1.00	<1.00	<1.00	<1.00	3
La	7	8	1	1	21	31	10
Ba	2060	6780	135	620	600	2060	580
Cr	12	27	20	19	7	8	36
Rb	32	67	13	16	29	23	170
Zr	465	475	522	488	466	759	621
Nb	23	32	22	23	39	42	24
Ce	170	33	67	86	116	110	291
Pr		1.4	0.3			0.5	
Nd		5	1			2	
Sm		1	0.3			0.3	
Eu		0.5	0.1			0.2	
Gd		1.6	0.3			0.5	
Tb		0.1	0.1			0.1	
Dy		0.5	0.2			0.2	
Ho		0.1	0.1			0.1	
Er		0.2	0.1			0.1	
Tm		0.1	0.1			0.1	
Yb		0.2	0.1			0.2	
Lu		0.1	0.1			0.1	
∑REE		51.8	70.8			145.4	
$(Eu/Eu^*)_{cn}$		1.21	1.02			1.58	
$(Ce/Ce^*)_{cn}$		1.01	0.91			1.32	
$(La/Sm)_{cn}$		8.19	2.1			4.19	
$(La/Yb)_{cn}$		43.82	6.74			6.74	
$(La/Lu)_{cn}$		419.35	32.26			64.52	
$(Eu/Sm)_{cn}$		1.33	0.88			1.77	
$(Gd/Yb)_{cn}$		6.46	2.42			2.02	
$(Tb/Yb)_{cn}$		2.2	4.41			2.2	
$(Tb/Lu)_{cn}$		0.68	0.68			0.68	

$Eu/Eu^* = Eu_N / \sqrt{(Sm_N\ Gd_N)}$ and $Ce/Ce^* = 3Ce_N / (2La_N + Nd_N)$ (Mongelli, 1997). LOI: Loss on ignition at 1050 °C.

Table 2. Semiquantitative analyses of the Yenipazar (Yozgat) clay deposits.

Sample	Kaolinite	Halloysite	Smectite	Mixed-layer	Illite/mica	Quartz	Chlorite	Feldspar	Calcite	Alunite	Jarosite	Pyrite	Hematite
YPD6-2	+ -		x		+	+ + x		ac	ac				
YPD6-3	+ -		x		+	+ + x		ac	ac				
YPD6-4	+ -		x		+	+ + x		ac	ac				
YPD6-10	+ + -		-	-		+ -				ac			
YPD6-11		+ + + + -	-			ac							
YPD6-11A		+ + + x	+ x		-	ac							
YPD6-13		+ + + - x		-	x	-			ac	ac			
YPD6-13A		+ + + - x		-	x	-			ac	ac			
YPD6-14	+ + - x		x		-	+	x		ac	x			
YPD6-15	+ + - x		x		-	+	x		ac	x			
YPD6-17			x		+ + x	+ -	+						
YPD6-18			x		+ + x	+ -	+						
YPD6-19			x		+ + x	+ -	+						
YPD6-20			x		+ + x	+ -	+						
YPD6-21	x				+ + +	- x	-	x		ac		x	ac
YPD6-22	x				+ + +	+ x	-	x		ac		x	ac
YPD6-23	x				+ + - x	+ x	-	x		ac		x	x
YPD6-26			x		+ + - x	+	- x	x		ac		ac	
YPD163-3	+ + x			x	+	+	-	ac		ac	ac		
YPD163-4	+ + x			-	+	-	- x	ac		ac	ac		
YPD163-5	+ + + - x		-		x	x		ac		x			
YPD163-7	+ + -		- x		+	- x							ac
YPD163-8	+ + - x		- x		+	-							
YPD140-1	+ +		+		- x	+	x			ac			
YPD140-2	+ - x		+	-	-	-				ac	ac		-x
YPD140-2a	+ +		+	x	- x	+				ac	ac		ac
YPD140-3	-		+ + -		- x	+				x	ac		ac
YPD140-4	- x		+ -		+ -	+ x		ac		ac			ac
YPD140-5	-		+ -		+ -	+ -		ac		ac			ac

Table 2. (Continued.)

Sample	Kaolinite	Halloysite	Smectite	Mixed-layer	Illite/mica	Quartz	Chlorite	Feldspar	Calcite	Alunite	Jarosite	Pyrite	Hematite
ES4-1	+ +		- x		-	+		x	-				
ES4-2	+ +		- x		-	+		x	-				
ES4-4	- x		+		-	+ x		+ -					
ES4-5	- x		+		-	+ x		+ -					
ES4-5a	- x		+		-	+ x		+ -					
ES4-6				+ x	+ - x	+ x	-	ac	ac			x	
ES4-6a				+ x	+ - x	+ x	-	ac	ac			x	
ES4-7			+		+ + x	+	- x	ac	ac				ac
ES4-8			+		+ + x	- x	- x	ac	ac				x
YPD76-2	+ +		+ x		- x	x		x					-
YPD76-3	+ x		+ - x		- x	-	-	ac		ac			x
ES3-1	+ + +		-		-	-		-		ac	ac		
ES3-2	+ -	+ x	-		+ -	x				ac	ac		
ES3-3		+ x	+ + -		x	+		ac	ac				
ES3-4		+ x	+ + -		x	+		ac	ac				
ES3-5	x		-	-	+ x	+ x	- x	x	ac	ac		ac	x
ES3-6			-	-	+	+ -	+ x	x		ac			ac
ES3-7			-	-	+	+ -	+ x	x		ac			ac

+: approximately 20 wt.%, - : approximately 10 wt.%, x: approximately 5 wt.%. ac: accessory. Goethite- and serpentine-group minerals were observed only in sample YPD140-2 and sample 140-3 as accessory minerals, respectively. Low cristobalite was only observed in samples YPD6-13A and YPD6-17 and barite was only observed in samples YPD76-2 and YPD76-3 as an accessory mineral.

low cristobalite in lesser amounts, the SiO_2 values of clays reach up to 66.1%.

6. Discussion: origin of clay deposits

Since kaolinite and halloysite are the dominant clays in the clay deposits, it is thought that kaolinization was a predominant process persisting in all alteration cycles. In this study, kaolinization occurs by the reaction of parent rock, mica schist, and gneiss, with hydrothermal solutions. During the Late Cretaceous volcanic activities, hydrothermal solutions that arose from magma most probably played an important role in the kaolinization process. In addition, meteoric water heated by contact with hot rocks adjacent to the magma chamber may have also played a role. Einarsson (1942) proposed that the heating of meteoric water in contact with magma heated country rocks is the predominant mechanism. An increased geothermal gradient due to the graben tectonism could be the heat source for the Emet geothermal field (Gemici et al., 2004). A role of heated meteoric water for the formation of the Hisarcık kaolin deposits was also accepted by Sayın (2007). Hydrothermal fluids that originated as meteoric water are the only altering agents for the formation of metamorphic hosted clay deposit (pyrophyllite and dickite) in Pütürge, Malatya, central eastern Turkey during the Cretaceous and later times (Bozkaya et al., 2007). The absence of pyrophyllite within the studied clay deposits suggests the lower-temperature parts of the hydrothermal stage of hypogene conditions. Thus, it is thought that the altering acidic solution that was tectonically controlled and resulted in the development of clay deposits has been active after the formation of VMS deposits.

The origin of kaolin is discussed in the following subsections, namely fractures, mineral paragenesis, silica zones (silica gossan), trace elements, REEs, and textures of clays.

6.1. Fractures

After magmatic activities in the Late Cretaceous and Paleocene, orogenic cycles with compression and extensions dominated in the region (Bayhan and Tolluoğlu, 1987; Kurt et al., 1991). As a result of the extensional and compression tectonic regime, a series of grabens and transform faults occurred in the region (Kurt et al., 1991). In the study area, in the northeast of the ore mineralization area, a normal fault trending in a northeast-southwest direction is present as a border between marble and mica schist. On the other hand, four parallel faults trending in the northwest-southeast direction have been observed during drilling activities and all core sample investigations of the mineralized zone. A tear fault cutting across the ore mineralization zone with about northwest-southeast direction has developed after the ore mineralization zone and clay occurrences (Figure 1). It is assumed that the activity of volcanism may have been more intense due to extensional tectonics. Consequently, hot solutions related to this magmatic activity may have been associated with the fault systems most probably in a northwest-southeast direction. In addition, the observation of several alteration levels from the boreholes emphasizes that some secondary crack systems also developed, most probably parallel to these fault systems. Thermal solutions mainly of magmatic origin most probably ascended along these fault zones and crack systems within the quartz mica schist and gneiss. Moreover, circulative hot meteoric waters might have also caused clay alteration in the study area.

6.2. Mineral paragenesis and silica zones (silica gossan)

No clay outcrops have been observed in the study area. In other words, alteration zones related to the clay deposits are not visible in the field. All studies on clays are based on drillings activities. The formation of kaolinite in the system of Na_2O-K_2O-Al_2O_3-SiO_2-H_2O depends on the alkali/H^+ activity ratio (Hemley and Jones, 1964). If the removal of dissolved K^+, Na^+, and Ca^{+2} occurs rapidly, kaolinite forms directly from K-feldspar and plagioclase (strong hydrogen metasomatism). This environment requires a very low alkali and calc-alkali ions/H^+ activity ratio. The alteration of plagioclase and K-feldspar results in smectite (mainly montmorillonite) and/or mixed layer smectite/illite, if alkali and calcic ions are present within the solution. If the K^+/H^+ activity ratio of the solution is low, probably due to low pH, kaolinite instead of the illite/smectite mixed layer is favored (Christidis, 1995). The temperature of the solution may also play a role in the removal of the alkali and calc-alkali cations from solution. On the other hand, the Si/Al ratio of a hydrothermal system also plays an important role in kaolinite synthesis (Eberl and Hower, 1975). According to these authors, if the atomic Si/Al ratio is less than 2.0, kaolinite will persist. However, all boreholes have similar patterns and suggest a typical vertical alteration zones, as follows: i) Intense hydrogen metasomatism (strong kaolinization) of the feldspar representing lower cation/H^+ ratios persisted in the upper section of the clay bodies, since kaolinite and halloysite are the dominant clay minerals within the strong acidic condition. ii) Smectite and illite are predominant in the lower part of the clay bodies, representing high cation/H^+ ratios (weak kaolinization) (Figures 3 and Figure 7). iii) Chlorite, muscovite, and feldspar are dominant at the bottom of the clay bodies, representing relatively higher cation/H^+ ratios (weakly clayey level). Here, kaolinite, smectite, and illite are present in minor amounts. This weakly clayey level passes into the slightly altered quartz mica schist and gneiss (parent rocks). iv) The silica zone (silica gossan) is at the top of the clay bodies (kaolin deposit). The samples taken from boreholes YPD71 and ES1 in the north and YPG09 and YPD152 in the south, which were opened

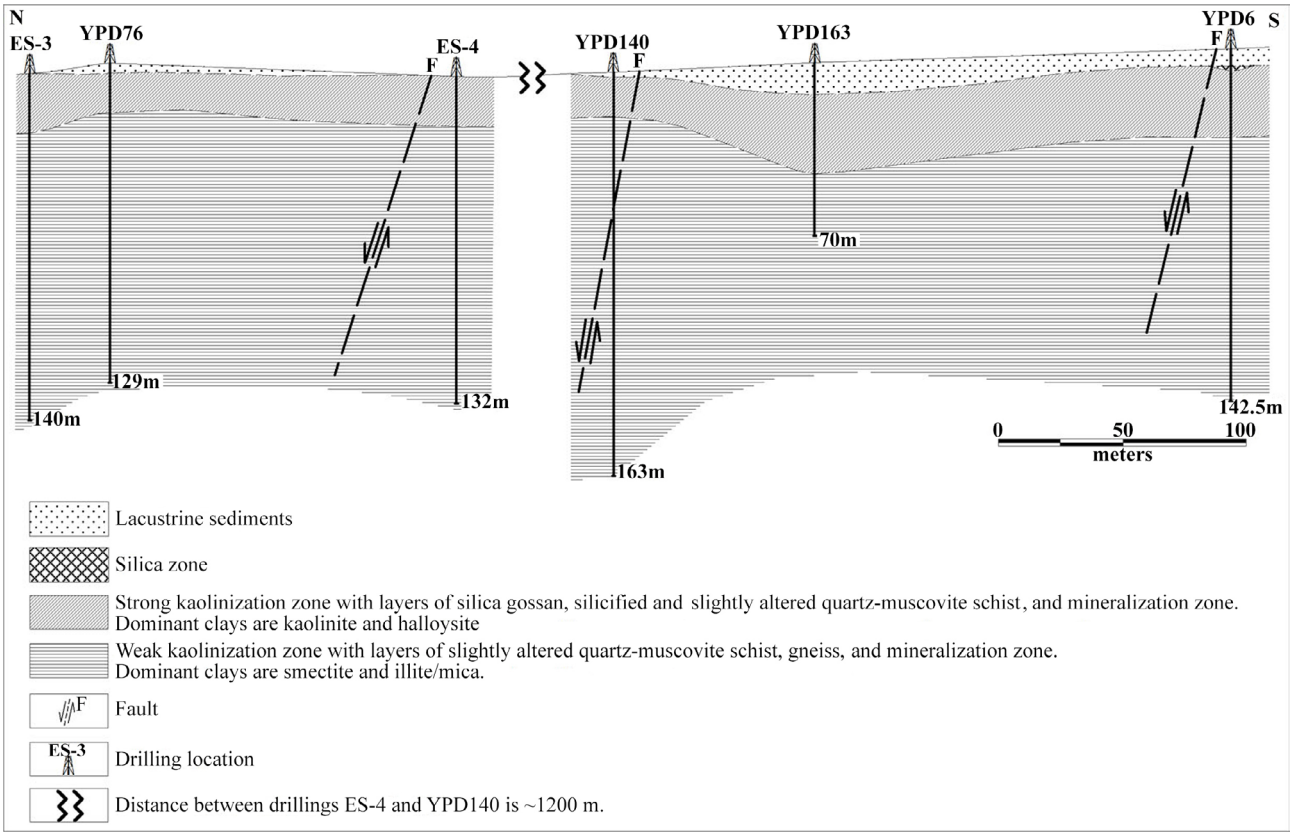

Figure 7. Schematic geological profile of Yenipazar clay deposits showing alteration zones.

at the east and west side of the clay bodies, also indicate a lateral mineralogical zonation. These samples, which represent outer zones, consist mainly of chlorite, quartz, feldspar, smectite, and illite. Reyes (1991), Sayın (1984, 2001, 2004, 2007), and Hedenquist et al. (1996) observed typical mineralogical zonation with a kaolinite and alunite zone in the center and smectite and illite-bearing outer zone in the hydrothermal deposits. Mineralogical zonation from the main kaolin deposits outwards at the Kütahya kaolin deposits are as follows: kaolinite + smectite + illite + opal-CT + feldspar (Kadir et. al., 2011). Due to very intense H-metasomatism (strong kaolinization) as seen in Kohdachi (Japan), the kaolin deposit contains three alteration zones: 1) halloysite zone, 2) halloysite + kaolinite zone, and 3) kaolinite zone (Kitagawa and Koster, 1991). In particular, the presence of a silica zone (silica gossan) overlying the kaolin occurrences clearly indicates the presence of hypogene altering solutions. Typical silica gossans are present in hydrothermal kaolin deposits in Japan (Iwao, 1968), Mexico (Keller and Hanson, 1968, 1969), and Turkey (Sayın, 1984, 2004, 2007; Ece et. al., 2013). Silica derived mainly from parent rocks (here, mica schist and gneiss) and/or the magmatic solution itself was concentrated within the rising solution. Because of sudden temperature drop, dissolved silica in the solution precipitated on the kaolin deposit forming the silica zones. As seen in borehole ES4, the dissolved silica may also replace and silicify the altered quartz muscovite schist. Similar upwards silicifications are quite widespread in the western Peru kaolin deposits (Dill et al., 1997).

Mica schist, gneiss, and clay deposits all contain some pyrite. The breakdown of pyrite under the condition of strong H-metasomatism may easily create a sulfate-rich solution, and the formation of alunite from this type of solution is expected. Consequently, the presence of alunite and jarosite within the kaolin deposits is quite widespread. The frequent association of kaolinite and alunite is to be expected on the basis of phase equilibrium data for both hot solutions and higher temperature environments (Hemley et al., 1969). Here, they point out that rather high acidity is definitely needed in an equilibrium silicate–alunite system at the elevated temperatures involved in their experimentation. Alunite group minerals are often formed under acid oxidizing conditions in hypogene porphyry Cu and epithermal Au deposits (Knight, 1977). Scott (1990) also emphasized that K- and Na-rich members of the alunite group form as hydrothermal minerals in the acid-sulfate epithermal system. He concluded that jarosite

formed either by replacement of alunite or directly from pyrite.

6.3. Trace elements

The results of representative trace elements and REEs of the parent rocks (fresh and slightly altered muscovite schist) and clay deposits are given in Table 1. The parent rocks and clay deposits have very low V, Co, Ni, Cr Se, Y, and Cd contents. The Ba contents, which are associated with barite mineral, vary from 135 ppm to 25,700 ppm in the clay deposits. Ba, Pb, Zn, and Cu are more common in the clay deposits than in the parent rocks, since kaolinization may have taken place after the formation of VMS orebody and the hot corrosive solutions should have been enriched with some dissolved Ba, Pb, Zn, and Cu when passing through the ore body. Sr contents within the clays, which vary from 177 ppm to 528 ppm, are closely associated with Ca- or K-bearing minerals, namely feldspar, mica, illite, smectite, and alunite. Dill et al. (1997) observed Pb enrichment within the hydrothermal kaolin deposits hosted by volcanic rocks in Peru. Beeson (1980), Sayın (2007), and Cravero et al. (2010) also pointed out Pb and Sr enrichments within the hydrothermal kaolin zones at Sarkhanlu (northwest of Iran), Hisarcık (western of Turkey), and Patagonia (Argentina), respectively. Rb is directly related to K and was removed during the strong kaolinization process. Therefore, the clay deposits have a Rb content lower than that of their parent rocks. The low Nb contents in both parent rocks and clay deposits are concentrated in Ti minerals. The clay deposits contain higher Zr contents than those seen in the parent rocks. Zr is more likely to be related to the presence of accessory zircon in the clay deposits. Zr concentration in the clay deposits may also be due to the absorption phenomena of finest clay particles (Wiewiora, 1978).

High Pb, Zn, Cu, Ba, Sr, and Zr and low Cr, Nb, Ti, Ce, Y, and La values in the Yenipazar clay deposits suggest a hypogene origin, similar to the Lohreim kaolinite deposit (Dill et al., 1995) and the Karaçayır kaolinite deposit (Kadir and Erkoyun, 2012).

On the Zr vs. TiO_2, Cr + Nb vs. Fe + Ti, and Ba + Sr vs. Ce + Y + La diagrams (Dill et al., 1997; Ece et. al., 2013), plots of the Yenipazar clay samples appear to be comparable to the hypogene Lastarria kaolinites of Peru and the Karaçayır metamorphic kaolinites (Kadir and Erkoyun, 2012) (Figure 8).

In general, the degree of kaolinization, the mineral paragenesis within the clay occurrences, and the chemistry of the hot corrosive solutions passing through the country or parent rocks could all have affected the distribution of trace elements within the clay deposits. On the other hand, the attraction of the trace elements to the clay surface would be different for each element. However, it may be concluded that the absorption phenomena of the

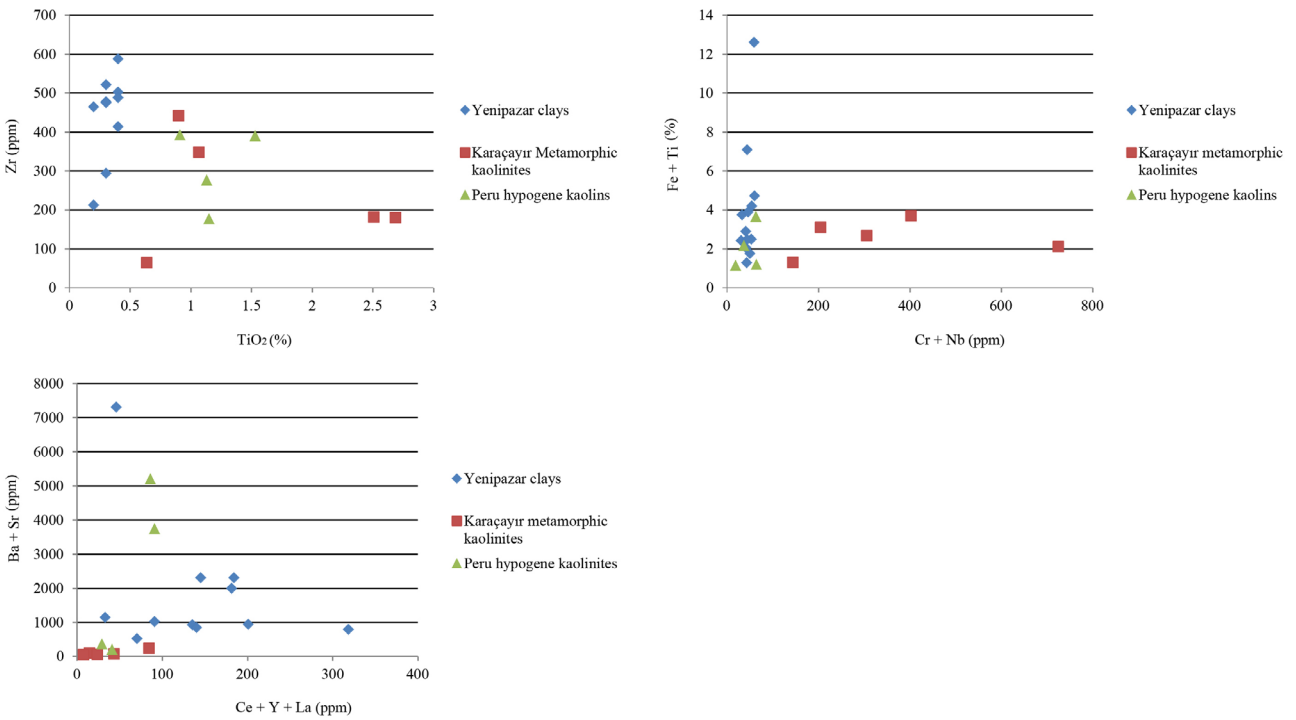

Figure 8. Genetic analysis of the Yenipazar clay samples using Zr vs. TiO_2, Cr + Nb vs. Fe + Ti, and Ba + Sr vs. Ce + Y + La diagrams of Dill et al. (1997).

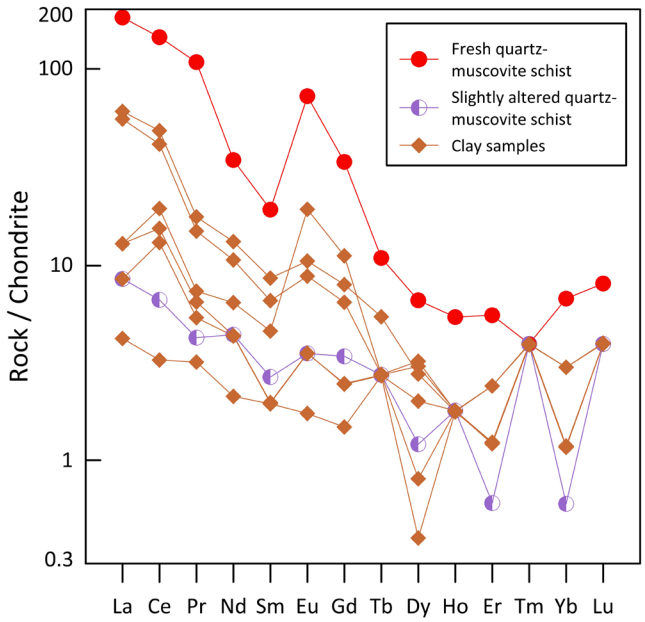

Figure 9. Chondrite-normalized REE patterns (Boynton, 1984) for clays and related parent rocks of the Yenipazar area.

clay crystals (mainly kaolinite) could be an influence in the enrichment of Cu, Pb, Zn, Sr, Zr, and Ba in the clay deposits.

The REEs were normalized to chondrite values (Figure 9). The REE patterns display an enrichment of LREEs [$(La/Sm)_{cn}$ = 2.10–8.19 and $(La/Lu)_{cn}$ = 32.26–451.61], a depletion of HREEs [$(Gd/Yb)_{cn}$ = 2.02–6.46, $(Tb/Yb)_{cn}$ = 0.88–4.41, and $(Tb/Lu)_{cn}$ = 0.68–1.36], and positive Eu anomalies [(Eu/Eu^*) = 1.02–2.65, $(Eu/Sm)_{cn}$ = 0.88–4.17, and (Ce/Ce^*) = 0.91–1.47] in clay samples. The positive Eu anomalies may reflect the presence of Ca-plagioclase and calcite. The positive Ce anomalies suggest a high content of Zr.

6.4. Textures of clays

SEM micrographs of the clay crystals are discussed as follows. Due to very tight packing, all kaolinite (book-type) and halloysite (tube-type) crystals exhibit a low porous texture. Keller and Hanson (1975) and Sayın (1984, 2007) suggested that higher rock pressure due to overburden may create very low porous texture in the hydrothermal kaolin deposits. The very small kaolinite crystals (0.5 μm) appear to have been formed from the in situ breakdown of the rosette-type structure of smectite. This suggests a phase transition between smectite and kaolinite. This also explains that smectite and/or illite are the first clay minerals formed at the beginning of H metasomatism of mica schist and gneiss, mainly from feldspar crystals as a result of the dissolution–precipitation mechanism. Similar phase transitions between montmorillonite and kaolinite were also observed by Keller (1976) and Sayın (1984, 2007). Montmorillonite and mica were converted into kaolinite by a H^+ ion-dominated altering solution (Kukovsky, 1969). According to Exley (1976), the formation of kaolinite is directly related to the destruction of montmorillonite and mica in authigenic systems. The transformation of smectite into mixed-layer kaolinite/smectite and kaolinite in the Paris basin clays were clearly observed by high-resolution transmission electron microscopy (Amouric and Olives, 1998). The presence of small kaolinite crystals in the cluster of halloysite tubes also suggests a phase transition between halloysite and kaolinite. The in situ phase transition between halloysite and kaolinite within intense H metasomatism systems is a well-known phenomenon (Sayın, 1984).

7. Conclusion

Associated with the tectonic framework, which consists of orogenic cycles with compression and extension after Late Cretaceous magmatic activities, kaolinite and halloysite dominated clay occurrences, mainly in the upper section of the clay deposits, that formed from the quartz mica schist and gneiss host rocks within the Yenipazar (Yozgat) VMS ore body in the Yenipazar district. The kaolinization process appears to have occurred postgenetically in regard to the VMS ore body and to have been controlled mainly by the fault systems oriented in the NW-SE direction in the investigated area. High Pb, Zn, Cu, Sr, Ba, and Zr and low Cr, Nb, Ti, Ce, Y, and La values in the clay deposits are consistent with a hypogene origin. Development of silica

zones (silica gossan) and silification of the parent rocks in the upper part of the clay deposits and the occurrence of sulfide and sulfate phases as goethite, pyrite, alunite, and jarosite support the idea of the presence of hydrothermal alteration. In addition, both vertical and horizontal mineralogical zonations suggest that hydrothermal alteration is the main cause for the development of the kaolin occurrences in the region. Depletion of both total REEs and HREEs as well as the enrichment of LREEs in clay deposits relative to their fresh host rocks suggests the lower-temperature parts of the hydrothermal stage of hypogene condition. Low positive Eu and Ce anomalies in the samples indicate some feldspar and Zr crystals in the clay deposits, respectively. SEM studies suggest that the transformation of smectite into kaolinite would increase with the intense kaolinization process. The development of kaolinite, either as book-type or tiny crystals, within the altered schist and gneiss records in situ precipitation, derived via a mechanism of both dissolution and precipitation. Despite the fact that no clay outcrops occur in the study area, the borehole sample investigations clearly reveal the concentration of two main clay occurrences in the northern (clay deposit A) and in the southern (clay deposit B) part of the mineralization zone with approximately 400 m and 550 m lengths, respectively. This was most probably due to the distribution of channel ways for corrosive hot solutions. The core sample investigation indicated that clay deposits consist of several clay veins with irregular boundaries depending on the tectonic framework.

Acknowledgments

The author thanks Aldridge Minerals, Inc. for financial support. The author also wishes to thank the staff of the Mineralogical and Chemical Analyses Laboratories of MTA, particularly Dr M Albayrak and S İçöz for XRD studies. The author is much indebted to the Coordinator of the Mineral Analyses Laboratory of MTA, O Zimitoğlu, for SEM studies. The author also thanks E Öner, IT officer of Aldridge Minerals, Inc., and I Ömeroglu for their help in preparing the manuscript.

References

Akyürek B, Bilginer E, Akbaş B, Hepşen N, Sunu D, Soysal Y, Dağer Z, Çatal E, Sözeri B, Yıldırım H et al. (1984). Ankara-Elmadağ-Kalecik dolayının temel jeolojik özellikleri. Jeol Müh 20: 31–46 (in Turkish).

Amouric M, Olives J (1998). Transformation mechanism and interstratification in conversion of smectite to kaolinite: an HRTEM study. Clay Clay Miner 46: 5 521–527.

Arni P (1938). Kırşehir kuzeybatısında bulunan Kortundağ-Baranadağ granitindeki lösit porfir damarlari: MTA Rapor No: 825. Ankara, Turkey: MTA (in Turkish).

Bailey EB, McCallien WC (1950). Ankara melanjı ve Anadolu şaryajı. MTA Mecmuası 40. Ankara, Turkey: MTA (in Turkish).

Bayhan H, Tolluoğlu AÜ (1987). Çayağazı siyenitoyidinin (Kirşehir kuzeybatısı) mineralojik-petrografik ve jeokimyasal özellikleri. HÜ Yerbilimler 14: 109–120 (in Turkish).

Beeson R (1980). The recognition of hydrothermal processes in the trace elements geochemistry of uranium and thorium-enriched tuffaceous rocks, northwest Iran. J Geochem Explor 19: 9–25.

Boynton WV (1984). Cosmochemistry of the rare earth elements: meteorite studies. In: Henderson P, editor. Rare Earth Element Geochemistry. Amsterdam, the Netherlands: Elsevier, pp. 63–114.

Bozkaya Ö, Yalçın H, Başıbüyük Z, Bozkaya G (2007). Metamorphic-hosted pyrophyllite and dickite occurrences from the hydrous Al-silicates deposits of the Malatya-Pütürge region, Central Eastern Anatolia, Turkey. Clay Clay Miner 55: 423–442.

Brindley GW (1980). Quantitative X-ray analysis of clays. In: Brindley GW, Brown G, editors. Crystal Structure of Clay Minerals and Their X-ray Identification. London, UK: Mineralogical Society Special Publications, pp. 441–458.

Christidis GE (1995). Mechanism of illitization of bentonites in the geothermal field of Milos Island Greece: evidence based on mineralogy, chemistry, particle thickness and morphology. Clay Clay Miner 43: 569–585.

Cravero F, Marfil SA, Maiza PJ (2010). Statistical analysis of geochemical data: a tool for discriminating between kaolin deposits of hypogene and supergene origin, Patagonia, Argentina. Clay Miner 45: 183–196.

Dill HG, Bosse HR, Henning KH, Fricke A (1997). Mineralogical and chemical variations in hypogene and supergene kaolin deposits in a mobile fold belt the Central Andes of northwestern Peru. Minerelium Deposita 32: 149–163.

Dill HG, Fricke A, Henning KH (1995). The origin of Ba-and REE- bearing alumino-phosphate minerals from Lohrheim kaolinitic clay deposit. (Rheinisches Sciefergebirge, Germany) Appl Clay Sci 10: 231–245.

Eberl D, Hower J (1975). Kaolinite synthesis: the role of the Si/Al and (alkali)/(H^+) ratio in hydrothermal systems. Clay Clay Miner 23: 301–309.

Ece ÖI, Ekinci B, Schroeder PA, Crowe D, Esenli F (2013). Origin of kaolin-alunite deposits in Smav Graben Turkey: timing styles of hydrothermal mineralization. J Volcanol Geothermal Res 255: 57–78.

Einarsson T (1942). Uber das Wesen Der Heissen Quellen Island. Visindafelag Islendinga 26: 1–89 (in German).

Erguvanlı K, Buchardt A (1954). Kırşehir doğusunun jeolojik etüdü hakkında rapor. MTA Rapor 2373. Ankara, Turkey: MTA (in Turkish).

Erkan Y (1975). Orta Anadolu masifinin güneybatısında (Kırşehir bölgesinde) etkili rejyonalmetamorfizmanın petrolojik incelenmesi. Thesis, Hacettepe University, Ankara, Turkey (in Turkish).

Erkan Y (1976). Kırşehir çevresindeki rejyonal metamorfik bölgede saptanan isogradlar ve bunların petrolojik yorumlanmaları. HÜ Yerbilimler 2: 53–54 (in Turkish).

Erkan Y (1977). Orta Anadolu masifinin güneybatısında (Kırşehir bölgesinde) etkili rejyonal metamorfizma ile amfibol minerallerinin bileşimi arasındaki ilişkiler. HÜ Yerbilimleri 3–12 (in Turkish).

Erkan Y (1978). Kırşehir masifinde granat minerallerinin kimyasal bileşimi ve rejyonal metamorfizma arasındaki ilişkiler. TJK Bül 21/1: 43–50 (in Turkish).

Erkan Y (1980). Orta Anadolu masifinin kuzeydogusunda (Akdağmadeni-Yozgat) etkili olan bölgesel metamorfizmanın incelenmesi. TJK Bül 23: 213–218 (in Turkish).

Erkan Y (1981). Orta Anadolu masifinin metamorfizması üzerine yapılmış çalışmalarda varılan sonuçlar. In: TJK 35. Bilimsel Kurultayı (İç Anadolu Jeolojisi) Sempozyumu (in Turkish).

Erkan Y, Tolluoğlu AÜ (1990). Ulusal Birinci Türkiye Jeotravers alanı içinde yer alan Kırşehir metamorfiklerinin, petrografik, stratigtafik, tektonik ve metamorfizma özelliklerinin incelenmesi. Ankara, Turkey: TÜBİTAK (TBAG - 832 Projesi) (in Turkish).

Exley CS (1976). Observation on the formation of kaolinite in the St. Austell Granite, Cornwall. Clay Miner 11: 51–63.

Gemici Ü, Tarcan G, Çolak M, Helvacı C (2004). Hydrochemical and hydrogeological investigations of thermal waters in the Emet area (Kütahya, Turkey). Appl Geochem 19: 105–117.

Göncüoğlu MC (1977). Geologie des westlichen Niğde Massivs. PhD, Bonn University, Bonn, Germany (in German).

Göncüoğlu MC (1981). Nigde masifinin jeolojisi. In: TJK 35. Bilimsel Kurultayı (İç Anadolunun Jeolojisi Sempozyumu) (in Turkish).

Gündoğdu MN (1982). Geological, mineralogical and geochemical investigation of the Bigadiç Neogene Sedimentary Basin. PhD, Hacettepe University, Ankara, Turkey.

Hedenquist JW, Izawa E, Arribas A, White NC (1996). Experimental gold deposits: styles, characteristics and exploration. Journal of the Society of Resource Geology Special Publication 1: 1–16.

Hemley JJ, Hostetler PB, Guide AJ, Mountjoy WT (1969). Some stability relations of alunite. Econ Geol 64: 599–611.

Hemley JJ, Jones WR (1964). Chemical aspects of hydrothermal alteration with emphasis on hydrogen metasomatism. Econ Geol 59: 538–569.

Iwao S (1968). Zonal structure in some kaolin and associated deposits of hydrothermal origin in Japan. Proceedings of 23rd International Geological Congress 14: 107–113.

Jacobs Minerals Canada, Inc. (2014). Technical report on the NI 43-101 Yenipazar optimization study, Yozgat Province, Turkey. Toronto, Canada: Jacobs Minerals.

Kadir S, Erkoyun H (2013). Genesis of the hydrothermal Karaçayır kaolinite deposit in Miocene volcanics and Palaeozoic metamorphic rocks of the Uşak-Gürün Basin, Western Turkey. Turk J Earth Sci 22: 444–468.

Kadir S, Erman H, Erkoyun H (2011). Mineralogical and geochemical characteristics and genesis of hydrothermal kaolinite deposits within Neogene volcanites, Kütahya (Western Turkey). Clay Clay Miner 59: 250–276.

Keller WD (1976). Scan electron micrographs of kaolin collected from diverse origin—III. Influence of parent material on flint clays and flint-like clays. Clay Clay Miner 24: 262–264.

Keller WD, Hanson RS (1968). Hydrothermal alteration of a rhyolite flow breccia near San Luis Potasi, Mexico. Clay Clay Miner 16: 223–229.

Keller WD, Hanson RS (1969). Hydrothermal argillation of volcanic pipes in limestone in Mexico. Clay Clay Miner 17: 9–12.

Keller WD, Hanson RS (1975). Dissimilar fabrics by scan electron microscopy of sedimentary versus hydrothermal kaolins in Mexico. Clay Clay Miner 23: 201–204.

Ketin İ (1963). 1/500 000 ölçekli Türkiye jeolojisi haritası, Kayseri paftası M.T.A. Enst. yayınları. Ankara, Turkey: MTA (in Turkish).

Kitagawa R, Koster HM (1991). Genesis of the Tirschenreuth kaolin deposit in Germany compared with the Kohdachi kaolin deposit in Japan. Clay Miner 26: 61–79.

Kukovsky EG (1969). Alteration process in clay minerals. Clay Miner 8: 234–237.

Kurt Z, Altun E, Keskin H, Şengün M, Sütçü Y, Tekin F, Özay R, Erkan M, Örçen S (1991). Boğazlıyan (Yozgat) dolayının jeolojisi. M.T.A. Der. Rapor 9424. Ankara, Turkey: MTA (in Turkish).

Mongelli G (1997). Ce-anomalies in the textural components of Upper Cretaceous karst bauxites from the Apulian carbonate platform (southern Italy). Chem Geol 140: 69–79.

Oczlon MS (2006). Terrane map of Europe. Heidelberg, Germany: Heidelberg University.

Reyes AG (1991). Mineralogy, distribution and origin of acid alteration in Philippine geothermal systems. Geological Survey of Japan Report 277: 59–66.

Sağıroğlu A (1984). Akdağmadeni (Yozgat) Kurşun-Çinko yataklarinda cevherleşme. Jeoloji Müh 21: 15–27 (in Turkish).

Sayın SA (1984). The geology, mineralogy, geochemistry and origin of the Yeniçağa Kaolinite Deposits and other similar deposits in Western Turkey. PhD, University of London, London, UK.

Sayın SA (2001). Hydrothermal kaolin occurrences of Sorkun Yaylası (Ankara-Güdül), Turkey. In: 10th International Clay Symposium, Selçuk University, Konya, Turkey (abstract).

Sayın SA (2004). The role of H-metasomatism in the hydrothermal kaolin occurrences, Gönen, Western Turkey. Key Eng Mat 264–268: 1379–1382.

Sayın SA (2007). Origin of kaolin deposits: evidence from the Hisarcık (Emet-Kütahya) Deposits, Western Turkey. Turk J Earth Sci 16: 77–96.

Scott KW (1990). Origin of alunite- and jarosite-group minerals in the Leyshon epithermal gold deposit, Northeast Queensland, Australia. Am Mineral 75: 1176–1181.

Seymen İ (1981). Kaman-Kırşehir dolayında Kırşehir masifinin stratigrafisi ve metamorfizmasi. TJK Bül 24/2 (in Turkish).

Seymen İ (1982). Kaman dolayında Kırşehir masifinin jeolojisi. Thesis, İstanbul Technical University, İstanbul, Turkey (in Turkish).

Seymen İ (1983). Tamadağ (Kaman-Kırşehir) çevresinde Kaman grubunun ve onunla sınırdaş oluşukların karşılaştırmalı tektonik özellikleri. TJK Bül 26/2 (in Turkish).

Seymen İ (1984). Kırşehir masifi metamorfitlerinin jeolojisi ve evrimi. In: TJK Yayını, Ketin Sempozyumu (in Turkish).

Tolluoğlu AÜ (1986). Orta Anadolu masifinin güneybatısında (Kırşehir yöresinde) petrografik ve petrotektonik incelemeler. PhD, Hacettepe University, Ankara, Turkey.

Whitney DL, Hamilton MA (2004). Timing of high-grade metamorphism in Central Turkey and the assembly of Anatolia. J Geol Soc London 161: 823–828.

Whitney DL, Teyssier C, Fayon AK, Hamilton MA, Heizler M (2003). Tectonic controls on metamorphism, partial melting and intrusion: timing and duration of regional metamorphism and magmatism in the Niğde Massif, Turkey. Tectonophysics 376: 37–60.